Applied Physics Letters ARTICLE pubs.aip.org/aip/apl

Origin of brittle behavior of doped PbTe-based thermoelectric materials

Cite as: Appl. Phys. Lett. **124**, 022104 (2024); doi: 10.1063/5.0185002
Submitted: 28 October 2023 · Accepted: 26 December 2023 ·
Published Online: 10 January 2024

Ilya V. Chepkasov,[1,2,a] Alexander G. Kvashnin,[1] Aleksandra D. Radina,[1] Nikita A. Matsokin,[1,3] Faridun N. Jalolov,[1] Dmitry G. Kvashnin,[4,5] Artem R. Oganov,[1] and Zinovi Dashevsky[6]

AFFILIATIONS

[1]Skolkovo Institute of Science and Technology, Bolshoy Boulevard 30, Bld. 1, Moscow 121205, Russian Federation
[2]Katanov Khakas State University, 90 Lenin pr., Abakan 655017, Russia
[3]Kintech Lab Ltd., 12, 3rd Khoroshevskaya St., Moscow 123298, Russian Federation
[4]Emanuel Institute of Biochemical Physics RAS, 4 Kosygin Street, Moscow 119334, Russia
[5]School of Chemistry and Technology of Polymer Materials, Plekhanov Russian University of Economics, 36 Stremyanny Lane, Moscow 117997, Russia
[6]Department of Materials Engineering, Ben-Gurion University of the Negev, Beer-Sheva, Israel

[a]**Author to whom correspondence should be addressed:** I.Chepkasov@skoltech.ru

ABSTRACT

Finding new efficient thermoelectric materials is a significant challenge for materials science. It is crucial to have a comprehensive understanding of material-property relationships to develop new materials successfully, given that minor structural or compositional changes can result in significant property changes. This paper extensively utilizes advanced theoretical approaches and investigates the impact of *n*- and *p*-type impurities on the mechanical characteristics of PbTe thermoelectric materials. *n*- and *p*-type doping of PbTe were studied using various techniques, including elastic tensor calculations, crystal orbital Hamilton population method, and local vibrational theory. Our findings reveal the specific ways in which doping type affects the material's mechanical properties. This information can aid researchers in optimizing PbTe doping strategies.

More than 70% of the global energy consumption is lost as waste heat released into the environment.[1] These heat losses can be transformed into electricity using thermoelectric generators (TEGs). Thermoelectric devices are used for solid-state refrigeration and energy conversion in bulk form.[2,3] To maximize performance of these devices, thermoelectric materials should be *n*- and *p*-doped with a typical charge carrier concentration $\sim 10^{20}$ cm^{-3}. On the other hand, a high concentration of dopant impurities introduces disturbances into the crystal structure, which ultimately affects the mechanical properties of the material. This parameter, along with the figure of merit, the so-called parameter ZT of the thermoelectric material, is very important for real energy applications: thermoelectric generators (TEGs). In TEGs, the active legs from *n*- and *p*-type effective thermoelectric material experience heavy mechanical stresses due to a difference in temperature up to 500–600 K on the ends of legs.[4–9]

Lead telluride PbTe is a well-known thermoelectric material showing high efficiency in the medium temperature range.[9–11] Over the past few decades, significant improvements in thermoelectric performance have been achieved in *p*-type and *n*-type PbTe.[12–16] In particular, a high figure of merit, ZT, of about 2.5 and 2, was achieved in *p*-type and *n*-type PbTe, respectively.[17–20] The main drawback of using *p*-type PbTe compared with *n*-type PbTe is its high brittleness that restricted its widespread use. In particular, previous works[21,22] showed that *n*-type PbTe has much greater bending strength and is more ductile than *p*-type PbTe.

Two hypotheses were proposed to explain the brittle behavior of *p*-type PbTe. The first one claims that stiffening in a material comes from heavy Σ valence band of PbTe. In particular, a heavy mass Σ band lies below the lighter valence band maximum in PbTe by 0.2 eV (corresponding to a temperature of 300 K).[23–25] Increased temperature leads to increased concentration of hole carriers that enhances the contribution of the Σ band to electronic transport, leading to an increased density of states (DOS), effective masses, and valley degeneracy.[23–25] A previous study[21] noted that hardness and hole effective mass both increased at the same carrier concentrations in Na-doped *p*-type PbTe and speculated that Σ-band contributions may stiffen the bonds.

The second hypothesis is that the brittleness of *p*-type PbTe arises from the solid solution strengthening by *p*-type dopant substitution. The addition of dopants with a large ionic size mismatching that of their host sites creates local strain. The strain field may strongly interact with dislocations, raising the stress needed to break dislocations free.[26,27] It was found that alloying of Na-doped PbTe (*p*-type) with Cd increases the hardness compared to PbTe doped with only Na.[26] However, doping of *p*-type with Sn leads to lower hardening of PbTe compared with Na-type doping.[21,22] These results support the first hypothesis because adding Sn to PbTe increases the L-Σ gap and reduces Σ contributions to transport, while Cd does the opposite.[28,29] However, Male *et al.*[30] showed that the brittleness of PbTe correlates with dislocation density. The authors noticed that Cu and Ag dopants in Pb-rich PbTe provide a unique example of brittleness in *n*-type PbTe, which may stem from a combination of low doping efficiency, high diffusivity, and highly strained defect environments in the *n*-type interstitial configuration.

In this work, we study the origin of brittle behavior of *n*- and *p*-type PbTe by using density functional theory (DFT), crystal orbital Hamilton population (COHP) method, local vibrational theory, etc. The obtained results offer insights into the mechanism of brittle behavior of PbTe due to doping by *p*- and *n*-type impurities.

All DFT calculations were performed by using the Vienna *ab initio* simulation package (VASP) with plane wave basis sets.[31–33] The Perdew–Burke–Ernzerhof parametrization for exchange-correlation functionals (PBE and PBEsol) were used.[34,35] Our convergence tests showed that an energy cutoff of 550 eV gives an excellent convergence on energies and forces. The electronic self-consistency threshold was set to 1×10^{-6} eV.

Crystal orbital Hamilton population (COHP) method was used to study the chemical bonding between atoms in doped PbTe. To extract information about chemical bonding from the electronic density of states (DOS) of a crystal, the crystal orbital overlap population (COOP), was used. Crystal orbital Hamilton population (COHP) is another function that we used, and its sign (opposite to that of COOP) distinguishes bonding states from antibonding.

COHP has allowed one to obtain the information about bonding and anti-bonding states in a simple manner. The mathematical form of the COHP is very similar to that of a projected DOS equation, but the density-of-state matrix is weighted by the Hamilton matrix elements. For a periodic crystal, it can be defined as follows:[36]

$$COHP_{AB}(\varepsilon) = \sum_{\nu \in A} \sum_{\mu \in B} COHP_{\mu\nu}(\varepsilon), \tag{1}$$

$$COHP_{\mu\nu}(\varepsilon) = \frac{2}{V_{BZ}} \int_{BZ} H_{\mu\nu}(k) \left\{ \sum_{j} c^{*}_{\mu j}(k) c_{\nu j}(k) \delta(\varepsilon - \varepsilon_j(k)) \right\} dk, \tag{2}$$

where $H_{\mu\nu}(k)$ is the Hamiltonian matrix in reciprocal space, $c_{\mu j}(k)$ are the expansion coefficients of the jth occupied crystal orbital with the energy $\varepsilon_j(k)$ in terms of Bloch functions numbered in the same way, as atomic orbitals, by the subscript μ or ν. Integration over k in the Eq. (2) is performed in the Brillouin zone (*BZ*) with the volume V_{BZ}.

In the course of this study, COHP calculations were carried out using the LOBSTER algorithm,[37] and further consideration of the contribution of each orbital to the total binding energy was carried out using the Dragon software package.

Local stretching force constants estimate the bond strength[38] and were determined by using the LModeA-nano plugin.[39] To determine the local stretching, the VASP package[33] was used together with the PAW method[40] with an $8 \times 8 \times 8$ Γ-centered Monkhorst–Pack[41] *k*-point grid. The kinetic energy cutoff was set to 700 eV, and all calculations were converged until the acting net forces were not greater than 0.001 eV/Å. Both kinetic energy cutoff and density of *k*-point grid were defined according to the convergence test. We tested denser *k*-point grids and higher energy cutoffs, but no significant modifications in the total energy and lattice parameters were observed. The Perdew–Burke–Ernzerhof functionals (PBE and PBEsol) with generalized gradient approximation (GGA) exchange-correlation[34] were used for calculations of stretching force constants of studied compounds. We considered pure PbTe supercell $12.88 \times 12.88 \times 12.88$ Å^3 (32 Pb atoms, 32 Te atoms) and the doped structure (one impurity atom per 64-atom cell, concentration of 4.67×10^{20} cm^{-3}). At the first step, all considered supercells were relaxed using the VASP package. Second, the structural displacements were created using the Phonopy package;[42] their force evaluations were calculated. Third, all results on the calculated forces were analyzed to obtain the Hessian matrix and force constants data. At the final step, optimized geometries and their force constants were utilized to obtain local force constants using the PyMOL visualization system. Local vibrational mode theory allows one to obtain the values of local stretching force constant for each pair of atoms to be derived from the full Hessian matrix $\mathbf{f}^x$[38] as

$$k^a_n = (\mathbf{d}_n(\Lambda)^{-1}\mathbf{d}^T_n)^{-1}, \tag{3}$$

where $\mathbf{d}_n$ and Λ are determined via $\mathbf{d}_n = \mathbf{b}_n\mathbf{C}$ and superscript T represents the matrix transpose. $\Lambda = \mathbf{C}^T\mathbf{f}^x\mathbf{C}$, $\mathbf{C}$ is the matrix collection of N_{vib} eigenvectors column-wise. In our study, we calculated local stretching force constants from the finite displacement method because our system is too expensive to compute the full Hessian matrix $\mathbf{f}^x$.

Male *et al.* reported[30] that PbTe degrades due to changes in its plasticity. We performed DFT calculations of mechanical characteristics of doped PbTe (*n*- and *p*-type) to determine the influence of dopant on plasticity and ductility. For *p*-type dopants, we chose Na, K, Ag, Cu impurities that substitute one Pb atom in the considered 64-atom cell. These types of dopants are often used to improve the thermoelectric *p*-type properties of PbTe.[21,43–45] *n*-type doping was simulated by using Bi and Sb (Pb substitution) and Br, Cl, and I (Te substitution). These dopants are routinely used to improve the thermoelectric *n*-type properties of PbTe.[46–50]

For all considered dopants, the Pugh–Pettifor[51] criterion was calculated as shown in Fig. 1. One can clearly see two isolated sets of data corresponding to *n*- (green circles) and *p*-type impurities (orange diamonds). Calculated values of the elastic constants and elastic moduli are presented in Table S1 in the supplementary material. The *n*-type impurities make PbTe more ductile, less susceptible to fracture. The ionic radius of the dopant does not affect[30] the ductility of the material because the difference between the Shannon radii of Pb and Na (*p*-type) or Bi (*n*-type) atoms is approximately −0.16 and −0.17 Å, as was shown by Male *et al.*[30]

The Bi, Sb (*n*-type) and Na, K (*p*-type) impurities that substitute the Pb atom in PbTe were chosen for further investigation of the

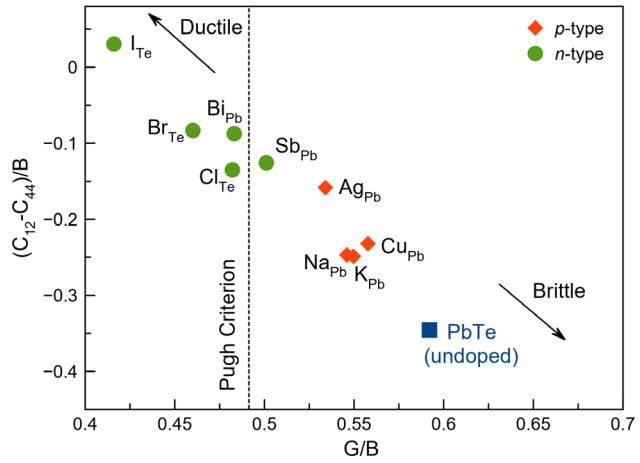

FIG. 1. Correlation between (C_{12}–C_{44})/B and G/B, where B is the bulk modulus, and G is the shear modulus. Top left points correspond to more ductile materials, while bottom right points correspond to more brittle ones. Pugh criterion was calculated for pristine PbTe.

mechanical properties in more detail. Figure 2(a) shows the considered supercells of undoped and doped PbTe. For these types of dopants, we have calculated the electron localization function (ELF), as indicated in Fig. 2(b). One can clearly see the deficiency of electrons in the *p*-type PbTe (Na and K) compared with *n*-type. Furthermore, from the charge density plotted for the conduction band minimum, one can see the additional electron density on the *n*-type dopants, as shown in Fig. S2 (see the supplementary material). It might be a key for understanding the brittle behavior of *n*-type and *p*-type doped PbTe.[52–56]

To understand the influence of dopants on the mechanical properties of the PbTe structure, we employed the local vibrational theory for local stretching force constants. As shown in Fig. 3, we virtually cut the 3D cell of the doped PbTe structure into two regions, namely A and B. Region A included the first atomic layer from the dopant in each direction. Region B surrounds the second atomic layer from the

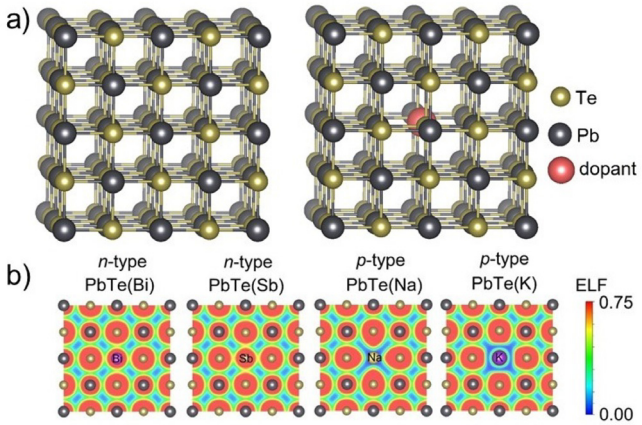

FIG. 2. (a) Crystal structure of considered supercells of undoped and doped PbTe. (b) Electron localization function of doped PbTe.

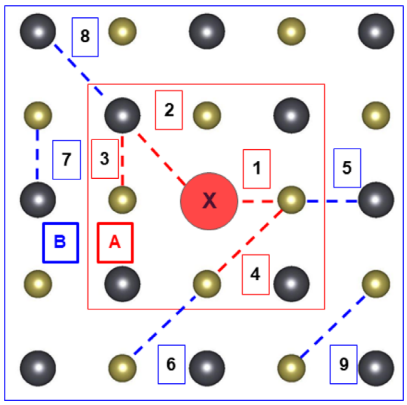

FIG. 3. Different interactions considered in the doped PbTe. The dopant atom and the interactions between the neighbors from the first atomic layer (denoted as A) are shown in red. The neighbors from the second atomic layer is highlighted by the blue square (denoted as B).

dopant, as demonstrated in Fig. 3. It is essential to quantify the evaluation of the dopant influence on the first-line atom and on the second one of the cell structure.

We selected four types of interactions (interactions 1, 2, 3, and 4 in Fig. 3) between atoms within the first atomic layer, denoted as A. Local stretching force constants, k_n^a, were calculated for considered interactions, summarized in Table S2 in the supplementary material. Presumably, the strongest influence of the dopant is observed for interaction between X and Te (interaction 1 in Fig. 3), since the distance between these atoms is the smallest. Local mode force constants of this interaction for Pb, Bi, Sb, Na, and K are 0.169, 0.153, 0.061, 0.141, and 0.314 mdyn/Å, respectively, (Table S5 in the supplementary material).

To compare local stretching force constants between interaction in the first and second atomic layers, we studied the next five interactions denoted as 5, 6, 7, 8, and 9 in Fig. 3. The calculated values of stretching force constants for these interactions are also shown in Table S5 in the supplementary material. We can assert that the substitution of Pb by dopant atoms demonstrates a much more significant influence in interaction 5, which refers to the Pb–Te bond located in the second atomic layer. There is the following order of dopants by their strength (k_n^a, mdyn/Å): K, Na (0.361, 0.228) < Pb (0.169) < Bi, Sb (0.129, 0.052).

For all dopants, the values of the ratios of the interaction from atomic layer A to atomic layer B were calculated to understand the qualitative influence (Fig. 3 and Table I). These ratios are crucially important. One can discover that Na and K doping increases stretching constants of interaction 5 by a factor of 1.62 and 1.15, respectively,

TABLE I. The ratios of stretching force constants from atomic layers A to B for all considered dopants.

Ratio	PbTe	$Bi_{Pb}(n)$	$Sb_{Pb}(n)$	$Na_{Pb}(p)$	$K_{Pb}(p)$
5 to 1	1.00	0.84	0.85	1.62	1.15
6 to 4	1.00	1.01	1.40	1.10	1.13
8 to 2	1.00	0.93	1.08	1.28	1.01

compared with interaction 1, see Table I. So, the *p*-type doping is dominated by ratios much greater than that for undoped PbTe for all considered interactions. It is worth noting that the *n*-type impurities behave qualitatively opposite to *p*-type ones. This directly correlates with the Pugh–Pettifor criterion, Fig. 1. The difference between short- and long-range bonding force constants in doped structures qualitatively defines the influence of *n*- and *p*-type metal impurities on the brittle behavior of PbTe. Comparison between stretching force constants calculated by using PBE and PBEsol functionals are shown in the supplementary material.

To comprehensively study the effect of strengthening, we calculated the crystal orbital Hamilton populations (COHPs). When PbTe is *p*-doped (Na, K), there is a hybrid interaction between the *s*-orbitals of the dopant and the *p*-orbitals of Te, resulting in the formation of a relatively strong bond [Figs. 4(a) and 4(d)], but still less strong than those found in pure PbTe. Sodium impurity leads to the shift toward bonding states at the Fermi level; see Fig. 4(b). Similar situation is observed for K in Figs. 4(d) and 4(f). However, since the *p* electrons need to decrease their energy to interact with the *s* electrons, such bonds are instantly destroyed if the energy is increasing because of some external influence (pressure or temperature). This explains the sharp brittle destruction of PbTe with *p*-type doping (e.g., Na[21]).

In the case of *n*-type doping (Sb, Bi) the *p* and *s* orbitals of the dopant atoms are partially filled with electrons, and Te electrons are forced to occupy the anti-bonding orbitals [Figs. 5(a) and 5(d)]. Similar results were obtained for Sb [Figs. 5(e) and 5(f)] where the interaction of the 5*p*-orbitals of Sb with the $5p_z$-orbitals of Te makes a significant contribution to the anti-bonding states. The same results were observed in the case of *n*-type PbTe when Te atom was replaced by atoms I, Br, and Cl (see Fig. S3 in the supplementary material). Thus, according to our analysis, we can conclude that the bond is weakened, while the material becomes more plastic and can better withstand various mechanical stresses with much smoother destruction than in the case of *p*-doped PbTe.

In conclusion, we performed a comprehensive study of the influence of *n*- and *p*-type impurities in PbTe thermoelectric material on the brittle behavior by employing density-functional calculations. Calculations of the correlations between $(C_{12}–C_{44})/B$ and Pugh modulus allowed us to state that *p*-doping leads to increase in brittleness of the material. Several dopants (Bi, Sb, Na, K) were then studied by using crystal orbital Hamilton population (COHP) and the local vibrational theory. These methods allowed us to obtain qualitative and quantitative results on the origin of the ductile behavior of *n*-type PbTe and the brittle behavior of *p*-type PbTe. The reason for the ductile behavior is the presence of an excess of electrons localized on the impurity atoms occupying the anti-bonding orbitals. This weakens the bond and the material becomes more plastic (more ductile). At the same time, our results showed the formation of stronger bonds in the case of *p*-type doping. This is caused by the fully occupied bonding orbitals in

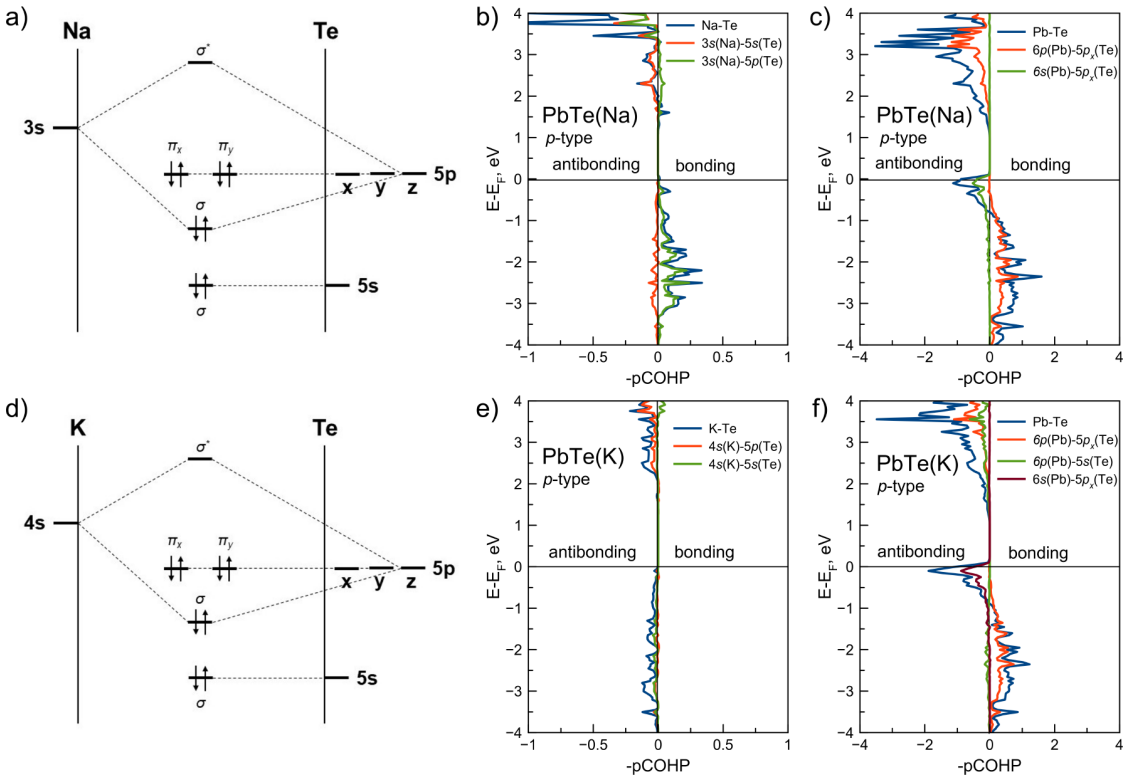

FIG. 4. (a) and (d) Electronic structure of the PbTe doped with the *p*-type dopant; (b) and (e) COHP diagrams for the interaction 1 between the dopant atom and the nearest Te atom; and (c) and (f) COHP diagrams for the interaction 5 on Fig. 3.

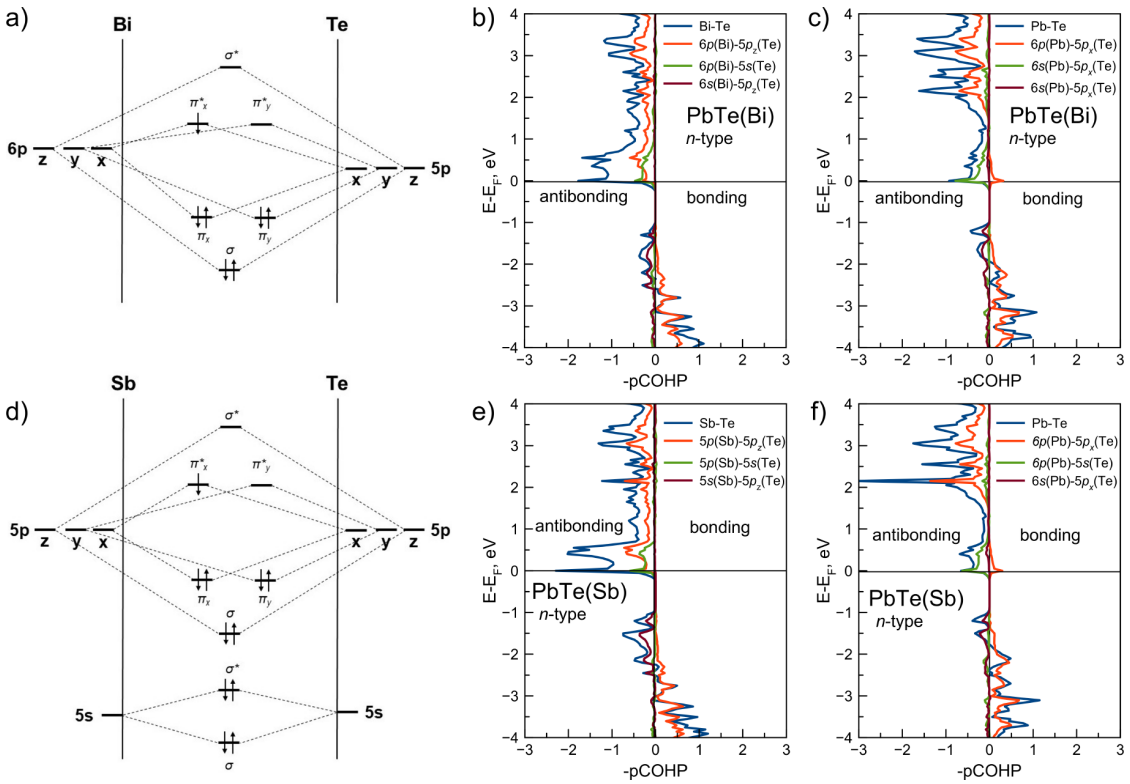

FIG. 5. (a) and (d) Electronic structure of the PbTe doped with the *n*-type dopant; (b) and (e) COHP diagrams for the interaction between the dopant atom and the nearest Te atom; and (c) and (f) COHP diagrams for the interaction 5 on Fig. 3.

the absence of anti-bonding. Our findings explain, from the chemical point of view, the emergence of weak interatomic bonds in PbTe and, in general, can be applied to other thermoelectric materials.

See the supplementary material for a description of calculations of local stretching force constants, elastic moduli, charge density, and COHP for the studied doped PbTe compounds.

The study was supported by the Russian Science Foundation under Grant No. 19-72-30043. The research was carried out using resources of the Center for the Information and Computing of Novosibirsk State University.

AUTHOR DECLARATIONS

Conflict of Interest

The authors have no conflicts to disclose.

Author Contributions

Ilia V. Chepkasov: Conceptualization (equal); Formal analysis (equal); Investigation (equal); Writing – original draft (lead); Writing – review & editing (equal). **Alexander G. Kvashnin:** Conceptualization (equal); Formal analysis (equal); Investigation (equal); Resources (equal); Supervision (equal); Writing – original draft (supporting); Writing – review & editing (equal). **Aleksandra D. Radina:** Investigation (equal); Methodology (equal); Writing – review & editing (supporting). **Nikita A. Matsokin:** Investigation (equal); Methodology (equal); Writing – review & editing (equal). **Faridun N. Jalolov:** Formal analysis (supporting); Investigation (equal); Methodology (equal); Writing – review & editing (supporting). **Dmitry G. Kvashnin:** Formal analysis (equal); Investigation (equal); Methodology (equal); Writing – review & editing (equal). **Artem R. Oganov:** Conceptualization (equal); Supervision (equal); Writing – review & editing (equal). **Zinovi Dashevsky:** Conceptualization (equal); Supervision (equal).

DATA AVAILABILITY

The data that support the findings of this study are available from the corresponding author upon reasonable request.

REFERENCES

[1]C. Forman, I. K. Muritala, R. Pardemann, and B. Meyer, "Estimating the global waste heat potential," Renewable Sustainable Energy Rev. **57**, 1568–1579 (2016).
[2]J. Wei, L. Yang, Z. Ma, P. Song, M. Zhang, J. Ma, F. Yang, and X. Wang, "Review of current high-ZT thermoelectric materials," J. Mater. Sci. **55**, 12642–12704 (2020).
[3]X. Yang, C. Wang, R. Lu, Y. Shen, H. Zhao, J. Li, R. Li, L. Zhang, H. Chen, T. Zhang *et al.*, "Progress in measurement of thermoelectric properties of micro/nano thermoelectric materials: A critical review," Nano Energy **101**, 107553 (2022).

[4]I. Petsagkourakis, K. Tybrandt, X. Crispin, I. Ohkubo, N. Satoh, and T. Mori, "Thermoelectric materials and applications for energy harvesting power generation," Sci. Technol. Adv. Mater. **19**, 836–862 (2018).
[5]Z. Dashevsky and S. Skipidarov, "Investigating the performance of bismuth-antimony telluride," in *Novel Thermoelectric Materials and Device Design Concepts* (Springer, 2019), pp. 3–21.
[6]M. A. Zoui, S. Bentouba, J. G. Stocholm, and M. Bourouis, "A review on thermoelectric generators: Progress and applications," Energies **13**, 3606 (2020).
[7]Z. Dashevsky, A. Jarashneli, Y. Unigovski, B. Dzunzda, F. Gao, and R. Z. Shneck, "Development of a high performance gas thermoelectric generator (TEG) with possible use of waste heat," Energies **15**, 3960 (2022).
[8]M. Maksymuk, B. Dzundza, O. Matkivsky, I. Horichok, R. Shneck, and Z. Dashevsky, "Development of the high performance thermoelectric unicouple based on Bi_2Te_3 compounds," J. Power Sources **530**, 231301 (2022).
[9]Z. Dashevsky, S. Mamykin, B. Dzundza, M. Auslender, and R. Z. Shneck, "A review of nanocrystalline film thermoelectrics on lead chalcogenide semiconductors: Progress and application," Energies **16**, 3774 (2023).
[10]Y. Xiao and L.-D. Zhao, "Charge and phonon transport in PbTe-based thermoelectric materials," npj Quantum Mater. **3**, 55 (2018).
[11]Y. Xiao and L.-D. Zhao, "Seeking new, highly effective thermoelectrics," Science **367**, 1196–1197 (2020).
[12]Y. Zhong, J. Tang, H. Liu, Z. Chen, L. Lin, D. Ren, B. Liu, and R. Ang, "Optimized strategies for advancing n-type PbTe thermoelectrics: A review," ACS Appl. Mater. Interfaces **12**, 49323–49334 (2020).
[13]C.-H. Su, "Design, growth and characterization of PbTe-based thermoelectric materials," Prog. Cryst. Growth Charact. Mater. **65**, 47–94 (2019).
[14]T. Parashchuk, B. Wiendlocha, O. Cherniushok, R. Knura, and K. T. Wojciechowski, "High thermoelectric performance of *p*-type PbTe enabled by the synergy of resonance scattering and lattice softening," ACS Appl. Mater. Interfaces **13**, 49027–49042 (2021).
[15]N. Mishra and G. Makov, "Point defects in lead sulfide: A first-principles study," Comput. Mater. Sci. **190**, 110285 (2021).
[16]K. T. Wojciechowski, T. Parashchuk, B. Wiendlocha, O. Cherniushok, and Z. Dashevsky, "Highly efficient n-type PbTe developed by advanced electronic structure engineering," J. Mater. Chem. C **8**, 13270–13285 (2020).
[17]G. Tan, F. Shi, S. Hao, L.-D. Zhao, H. Chi, X. Zhang, C. Uher, C. Wolverton, V. P. Dravid, and M. G. Kanatzidis, "Non-equilibrium processing leads to record high thermoelectric figure of merit in PbTe–SrTe," Nat. Commun. **7**, 12167 (2016).
[18]Y. Wu, P. Nan, Z. Chen, Z. Zeng, R. Liu, H. Dong, L. Xie, Y. Xiao, Z. Chen, H. Gu *et al.*, "Thermoelectric enhancements in PbTe alloys due to dislocation-induced strains and converged bands," Adv. Sci. **7**, 1902628 (2020).
[19]M. H. Lee, J. H. Yun, G. Kim, J. E. Lee, S.-D. Park, H. Reith, G. Schierning, K. Nielsch, W. Ko, A.-P. Li *et al.*, "Synergetic enhancement of thermoelectric performance by selective charge Anderson localization–delocalization transition in n-type Bi-doped PbTe/Ag_2Te nanocomposite," ACS Nano **13**, 3806–3815 (2019).
[20]Z.-Z. Luo, S. Cai, S. Hao, T. P. Bailey, X. Su, I. Spanopoulos, I. Hadar, G. Tan, Y. Luo, J. Xu *et al.*, "High figure of merit in gallium-doped nanostructured n-type PbTe-*x*GeTe with midgap states," J. Am. Chem. Soc. **141**, 16169–16177 (2019).
[21]Y. Gelbstein, Z. Dashevsky, and M. P. Dariel, "The search for mechanically stable PbTe based thermoelectric materials," J. Appl. Phys. **104**, 033702 (2008).
[22]Y. Gelbstein, G. Gotesman, Y. Lishzinker, Z. Dashevsky, and M. Dariel, "Mechanical properties of PbTe-based thermoelectric semiconductors," Scr. Mater. **58**, 251–254 (2008).
[23]A. D. LaLonde, Y. Pei, H. Wang, and G. J. Snyder, "Lead telluride alloy thermoelectrics," Mater. Today **14**, 526–532 (2011).
[24]H. Sitter, K. Lischka, and H. Heinrich, "Structure of the second valence band in PbTe," Phys. Rev. B **16**, 680 (1977).
[25]R. Allgaier, "Valence bands in lead telluride," J. Appl. Phys. **32**, 2185–2189 (1961).
[26]A. Crocker and M. Wilson, "Microhardness in PbTe and related alloys," J. Mater. Sci. **13**, 833–842 (1978).
[27]R. D. Shannon, "Revised effective ionic radii and systematic studies of interatomic distances in halides and chalcogenides," Acta Crystallogr., Sect. A **32**, 751–767 (1976).
[28]K. Ahn, K. Biswas, J. He, I. Chung, V. Dravid, and M. G. Kanatzidis, "Enhanced thermoelectric properties of p-type nanostructured PbTe–MTe (M = Cd, Hg) materials," Energy Environ. Sci. **6**, 1529–1537 (2013).
[29]E. M. Hedegaard, A. A. Mamakhel, H. Reardon, and B. Iversen, "Functionally graded $(PbTe)_{1-x}(SnTe)_x$ thermoelectrics," Chem. Mater. **30**, 280–287 (2018).
[30]J. P. Male, L. Abdellaoui, Y. Yu, S. Zhang, N. Pieczulewski, O. Cojocaru-Mirédin, C. Scheu, and G. J. Snyder, "Dislocations stabilized by point defects increase brittleness in PbTe," Adv. Funct. Mater. **31**, 2108006 (2021).
[31]G. Kresse and J. Furthmüller, "Efficient iterative schemes for *ab initio* total-energy calculations using a plane-wave basis set," Phys. Rev. B **54**, 11169 (1996).
[32]G. Kresse and D. Joubert, "From ultrasoft pseudopotentials to the projector augmented-wave method," Phys. Rev. B **59**, 1758 (1999).
[33]G. Kresse and J. Furthmüller, "Efficiency of *ab-initio* total energy calculations for metals and semiconductors using a plane-wave basis set," Comput. Mater. Sci. **6**, 15–50 (1996).
[34]J. P. Perdew, K. Burke, and M. Ernzerhof, "Generalized gradient approximation made simple," Phys. Rev. Lett. **77**, 3865 (1996).
[35]L. A. Constantin, J. M. Pitarke, J. Dobson, A. Garcia-Lekue, and J. P. Perdew, "High-level correlated approach to the jellium surface energy, without uniform-gas input," Phys. Rev. Lett. **100**, 036401 (2008).
[36]M. T. Ruggiero, A. Erba, R. Orlando, and T. M. Korter, "Origins of contrasting copper coordination geometries in crystalline copper sulfate pentahydrate," Phys. Chem. Chem. Phys. **17**, 31023–31029 (2015).
[37]V. L. Deringer, A. L. Tchougréeff, and R. Dronskowski, "Crystal orbital Hamilton population (COHP) analysis as projected from plane-wave basis sets," J. Phys. Chem. A **115**, 5461–5466 (2011).
[38]Y. Tao, W. Zou, D. Sethio, N. Verma, Y. Qiu, C. Tian, D. Cremer, and E. Kraka, "*In situ* measure of intrinsic bond strength in crystalline structures: Local vibrational mode theory for periodic systems," J. Chem. Theory Comput. **15**, 1761–1776 (2019).
[39]Y. Tao, W. Zou, S. Nanayakkara, and E. Kraka, "LModeA-nano: A pymol plugin for calculating bond strength in solids, surfaces, and molecules via local vibrational mode analysis," J. Chem. Theory Comput. **18**, 1821–1837 (2022).
[40]P. E. Blöchl, "Projector augmented-wave method," Phys. Rev. B **50**, 17953 (1994).
[41]H. J. Monkhorst and J. D. Pack, "Special points for Brillouin-zone integrations," Phys. Rev. B **13**, 5188 (1976).
[42]A. Togo and I. Tanaka, "First principles phonon calculations in materials science," Scr. Mater. **108**, 1–5 (2015).
[43]Z. Dashevsky, S. Shusterman, M. Dariel, and I. Drabkin, "Thermoelectric efficiency in graded indium-doped PbTe crystals," J. Appl. Phys. **92**, 1425–1430 (2002).
[44]Y. Takagiwa, Y. Pei, G. Pomrehn, and G. Jeffrey Snyder, "Validity of rigid band approximation of PbTe thermoelectric materials," APL Mater. **1**, 011101 (2013).
[45]H. Dow, M. Oh, B. Kim, S. Park, B. Min, H. Lee, and D. Wee, "Effect of Ag or Sb addition on the thermoelectric properties of PbTe," J. Appl. Phys. **108**, 113709 (2010).
[46]L. Fu, M. Yin, D. Wu, W. Li, D. Feng, L. Huang, and J. He, "Large enhancement of thermoelectric properties in n-type PbTe via dual-site point defects," Energy Environ. Sci. **10**, 2030–2040 (2017).
[47]L. Yang, Z.-G. Chen, M. Hong, L. Wang, D. Kong, L. Huang, G. Han, Y. Zou, M. Dargusch, and J. Zou, "n-type Bi-doped PbTe nanocubes with enhanced thermoelectric performance," Nano Energy **31**, 105–112 (2017).
[48]T. Parashchuk, I. Horichok, A. Kosonowski, O. Cherniushok, P. Wyzga, G. Cempura, A. Kruk, and K. T. Wojciechowski, "Insight into the transport properties and enhanced thermoelectric performance of *n*-type $Pb_{1-x}Sb_xTe$," J. Alloys Compd. **860**, 158355 (2021).
[49]Y. Dong, M. A. McGuire, A.-S. Malik, and F. J. DiSalvo, "Transport properties of undoped and Br-doped PbTe sintered at high-temperature and pressure ≥4.0 GPa," J. Solid State Chem. **182**, 2602–2607 (2009).
[50]I. Cohen, M. Kaller, G. Komisarchik, D. Fuks, and Y. Gelbstein, "Enhancement of the thermoelectric properties of n-type PbTe by Na and Cl co-doping," J. Mater. Chem. C **3**, 9559–9564 (2015).
[51]O. Senkov and D. Miracle, "Generalization of intrinsic ductile-to-brittle criteria by Pugh and Pettifor for materials with a cubic crystal structure," Sci. Rep. **11**, 4531 (2021).
[52]D. M. Ceperley and B. J. Alder, "Ground state of the electron gas by a stochastic method," Phys. Rev. Lett. **45**, 566 (1980).

[53]J. P. Perdew and A. Zunger, "Self-interaction correction to density-functional approximations for many-electron systems," Phys. Rev. B **23**, 5048 (1981).
[54]E. Mazhnik and A. R. Oganov, "A model of hardness and fracture toughness of solids," J. Appl. Phys. **126**, 125109 (2019).
[55]J. E. Ni, E. D. Case, K. N. Khabir, R. C. Stewart, C.-I. Wu, T. P. Hogan, E. J. Timm, S. N. Girard, and M. G. Kanatzidis, "Room temperature Young's modulus, shear modulus, Poisson's ratio and hardness of PbTe–PbS thermoelectric materials," Mater. Sci. Eng.: B **170**, 58–66 (2010).
[56]G. Li, U. Aydemir, B. Duan, M. T. Agne, H. Wang, M. Wood, Q. Zhang, P. Zhai, W. A. Goddard III, and G. J. Snyder, "Micro-and macromechanical properties of thermoelectric lead chalcogenides," ACS Appl. Mater. Interfaces **9**, 40488–40496 (2017).